ACS Catalysis

Research Article

pubs.acs.org/acscatalysis

Improved CO_2 Electroreduction Performance on Plasma-Activated Cu Catalysts via Electrolyte Design: Halide Effect

Dunfeng Gao,[†] Fabian Scholten,[†] and Beatriz Roldan Cuenya*[,†,‡]

[†]Department of Physics, Ruhr-University Bochum, 44780 Bochum, Germany

[‡]Interface Science Department, Fritz-Haber-Institut der Max-Planck Gesellschaft, 14195 Berlin, Germany

Supporting Information

ABSTRACT: As a sustainable pathway for energy storage and to close the carbon cycle, CO_2 electroreduction has recently gained significant interest. We report here the role of the electrolyte, in particular of halide ions, on CO_2 electroreduction over plasma-oxidized polycrystalline Cu foils. It was observed that halide ions such as I^- can induce significant nanostructuring of the oxidized Cu surface, even at open circuit potential, including the formation of Cu crystals with well-defined shapes. Furthermore, the presence of Cl^-, Br^-, and I^- was found to lower the overpotential and to increase the CO_2 electroreduction rate on plasma-activated preoxidized Cu catalyst in the order $Cl^- < Br^- < I^-$, without sacrificing their intrinsically high C_2−C_3 product selectivity (~65% total Faradaic efficiency at −1.0 V vs RHE). This enhancement in catalytic performance is mainly attributed to the specific adsorption of halides with a higher coverage on our oxidized Cu surface during the reaction, which have been previously reported to facilitate the formation and stabilization of the carboxyl (*COOH) intermediate by partial charge donation from the halide ions to CO_2.

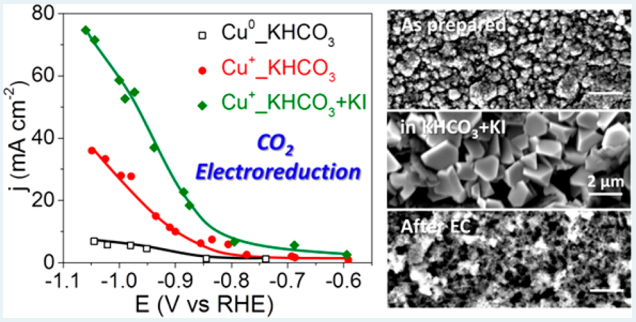

KEYWORDS: *CO_2 electroreduction, plasma treatment, electrolyte design, halide effect, C_2−C_3 products*

1. INTRODUCTION

Electrochemically converting CO_2 to chemicals and liquid fuels with high energy density by using water as the source of hydrogen is a promising pathway for the storage of renewable energy.[1−3] A variety of metallic catalysts have been identified to electrochemically reduce CO_2, but the major products that can be achieved with most metals are CO and formate.[4−7] Among them, Cu has attracted much attention due to its unique capability of producing hydrocarbons and alcohols in considerable amounts.[8] In order to overcome the high overpotential, low current density, and ethylene selectivity commonly observed on polycrystalline Cu electrodes,[4] nanostructured Cu catalysts have been designed to improve the activity and selectivity of CO_2 electroreduction.[9−26] The superior catalytic performances of these nanostructures are, among other factors, mainly attributed to the presence of an enhanced number of low-coordinated atoms,[9−11] grain boundaries,[12−14] Cu(100) facets,[15,16] increased roughness,[17] and the presence of subsurface oxygen and Cu^+ species.[18−23]

Apart from the ability to rationally design the electrode catalyst, tuning the nature and composition of the electrolytes will also affect the product distribution for CO_2 electroreduction.[27−48] Ionic liquids could serve as cocatalysts to promote the adsorption of CO_2 on the catalyst surface and reduce the energy barrier for CO formation.[27−30] Alkali-metal cations in aqueous solution are known to facilitate CO_2 adsorption and stabilize one of the possible intermediates, COOH*, through noncovalent interactions with adsorbed reagent species or field effect.[31−33] Hori et al.[34] found that ethylene formation became greater than that of methane with increasing cation size ($Li^+ < Na^+ < K^+ < Cs^+$). The variation of hydrocarbon selectivity was attributed to the difference in specific adsorption[34] or preferential hydrolysis[35] of different cations. The pH of the electrolyte, especially the local pH, plays a vital role in the activity and selectivity of CO_2 electroreduction.[36−39] On the other hand, anions also play an important role in product selectivity.[40−48] Formation of ethylene and alcohols is facilitated in KCl, K_2SO_4, $KClO_4$, and dilute $KHCO_3$ solutions, whereas methane is preferentially produced in relatively concentrated $KHCO_3$ and phosphate solutions.[40] The weaker buffer capacity of former anions would produce a high local pH at the electrode, which favors CO_2 reduction to ethylene and alcohols.[36,37] Bicarbonate (HCO_3^-) is considered to enhance the rate of CO_2 reduction to CO by increasing the effective concentration of dissolved CO_2 near the electrode surface through a rapid equilibrium between bicarbonate and dissolved CO_2.[41] Halides, the most extensively studied specifically adsorbed anions,[42] have been shown to enhance CO_2 reduction to methane by a covalent Cu−halide interaction[43,44] and increase in the negative charge on the

Received: May 1, 2017
Revised: June 16, 2017
Published: June 20, 2017

DOI: 10.1021/acscatal.7b01416
ACS Catal. 2017, 7, 5112−5120

surface.[45] Density functional theory calculations also confirmed the adsorption of Cl^-, Br^-, and I^- on Cu at potentials where CO_2 reduction is usually carried out.[46,47]

A plasma-activated Cu catalyst shows low overpotential and high ethylene selectivity,[18] but further improvement in the energy efficiency and reaction rate is still needed to render this process economically viable.[3,49] Inspired by the strong adsorption of halides on metal surfaces,[42−47] here we have studied the effect of halides on CO_2 electroreduction on plasma- oxidized Cu catalysts. It was observed that the presence of halides in the electrolyte further lowered the overpotential and led to an increase in the CO_2 electroreduction rate, without sacrificing the intrinsically high C_2-C_3 product selectivity typical of oxidized Cu systems. Although the role of the halides in the nanostructuring of the Cu surfaces was also considered and demonstrated, we will show here that the improved activity obtained is mainly attributed to the chemical effect of the adsorbed halides with a higher coverage on our oxidized Cu surface during the reaction, which are likely to contribute to the stabilization of the COOH* intermediate by donating partial charge from the halide ions to CO_2.

2. EXPERIMENTAL SECTION

2.1. Catalyst Synthesis. Commercial Cu foils (Advent Research Materials Ltd., 99.995%) were first cleaned with acetone and ultrapure water (18.2 MΩ) in an ultrasonic bath and then electropolished in phosphoric acid (VWR, 85 wt %) at 3 V versus a titanium foil for 5 min. The electropolished Cu foil was further treated in a plasma etcher (Plasma Prep III, SPI Supplies) at a gas pressure of 400 mTorr of O_2 and power of 20 W for 2 min.[18]

2.2. Surface Characterization. The morphology of the O_2-plasma-treated Cu foil was investigated by scanning electron microscopy (SEM) using a Quanta 200 FEG microscope from FEI with a field emitter as the electron source. The images were acquired under vacuum using a secondary electron (Everhart−Thornley) detector to ensure high surface sensitivity. An acceleration voltage of 10 keV and a working distance of 10 mm were found to yield the best balance among spatial resolution, surface sensitivity, signal to noise ratio, and field depth. A separate, liquid-N_2-cooled energy-dispersive X-ray spectroscopy (EDX) detector was employed for the elemental analysis of the sample. The content error bars for all the elements were made on the basis of the EDX spectra from at least ten different positions of two fresh samples. The samples after the reaction were washed thoroughly with water and transferred immediately to the SEM chamber in order to minimize air exposure. The amount of oxygen resulting from air exposure was negligible and did not affect the elemental analysis results, given that EDX with a probing depth of ∼300 nm at 10 keV is not surface-sensitive enough.

The quasi in situ X-ray photoelectron spectroscopy (XPS) measurements were carried out in an ultrahigh-vacuum setup equipped with a nonmonochromated Al X-ray source ($h\nu$ = 1486.6 eV) and a hemispherical electron analyzer (Phoibos 100, SPECS GmbH). The Cu $2p_{3/2}$ peak corresponding to CuO (933.11 eV)[50] was used for the energy alignment of the as-prepared plasma-oxidized sample. For the rest of the samples, which do not contain any Cu^{2+} species, the peak corresponding to Cu_2O (932.67 eV)[50] was used instead. The XPS analysis chamber was connected to an in situ electrochemical (EC) cell (SPECS GmbH). An Autolab potentiostat (PGSTAT 302N) was used for the electrochemical measurements. The sample transfer from the EC cell to the XPS ultrahigh-vacuum (UHV) chamber was performed under vacuum. All XPS spectra were acquired at room temperature. For the deconvolution of the Cu LMM Auger spectra, data acquired in our laboratory from a metallic Cu^0 foil (reduced *in situ* by H_2 plasma), freshly homemade CuI powders, and CuO and Cu_2O reference foils from the literature[51] were used as references. The Cu Auger spectra are more sensitive to the presence of Cu^+ species, in particular Cu_xO, in comparison to the O 1s spectra, because the latter are dominated by the contribution of adsorbed species not associated with Cu^+. They also allow us to distinguish Cu^+ from Cu^0, which is not the case when evaluating the Cu 2p XPS region.

2.3. Electrochemical Measurements. Electrochemical measurements were carried out in a gas-tight H-cell separated by a Nafion 211 membrane. Both, working electrode and counter electrode compartments were filled with 40 mL of electrolyte and purged continuously with CO_2 (20 mL min^{-1}). $KHCO_3$ (0.1 M; Sigma-Aldrich, 99.7%) was used as a reference and a buffer to avoid significant changes in the pH which could alter the reaction pathway for ethylene/methane formation.[36,37,45] The electrolytes were 0.1 M $KHCO_3$ or 0.1 M $KHCO_3$ + 0.3 M KX (X = Cl, Br, I) (Sigma-Aldrich, 99%). Prior to the measurement, the electrolyte was bubbled with CO_2 for 30 min to remove oxygen in the solution and saturate the solution. A platinum gauze (MaTecK, 3600 mesh cm^{-2}) was used as the counter electrode and a leak-free Ag/AgCl/3.4 M KCl electrode (Innovative Instruments, Inc.) as the reference electrode. The O_2-plasma-treated Cu foil was used as the working electrode and was contacted with a clamp wrapped by Kapton tape to avoid unwanted reaction. A fresh sample was measured with a chronoamperometric step for 1 h at each potential, unless stated otherwise. The potentials were controlled with an Autolab potentiostat (PGSTAT 302N). All potentials versus Ag/AgCl were converted to the reversible hydrogen electrode (RHE) scale and corrected for *iR* drop as determined by current interrupt. The roughness factors were determined by measuring double-layer capacitance with cyclic voltammetry between 0 and 0.25 V vs RHE in CO_2-saturated 0.1 M $KHCO_3$ solution (pH 6.8), after 1 h of CO_2 electroreduction in different electrolytes at −1.0 V vs RHE and thorough washing with water.[19]

2.4. Product Analysis. The gas products were analyzed by online gas chromatography (GC, Agilent 7890A) every 17 min. CO, H_2, and hydrocarbons were separated by different columns (Molecular sieve 13X, HayeSep Q, and Carboxen-1010 PLOT) and quantified by a thermal conductivity detector (TCD) and flame ionization detector (FID). Carboxylates (formate and acetate) formed during electrolysis were analyzed by high-performance liquid chromatography (HPLC, Shimadzu Prominence), equipped with a NUCLEOGEL SUGAR 810 column and refractive index detector (RID). Alcohols were analyzed with a liquid GC (Shimadzu 2010 plus), equipped with a fused silica capillary column and FID. An aliquot of the electrolyte after reaction was directly injected into the HPLC and liquid GC without further treatment. The reported Faradaic efficiency (FE) and production rate were calculated on the basis of the product distribution and current after 1 h of the reaction at constant potentials (see the Supporting Information).

3. RESULTS AND DISCUSSION

Our plasma-activated Cu catalysts were synthesized at room temperature by treating an electropolished polycrystalline Cu

DOI: 10.1021/acscatal.7b01416
ACS Catal. 2017, 7, 5112−5120

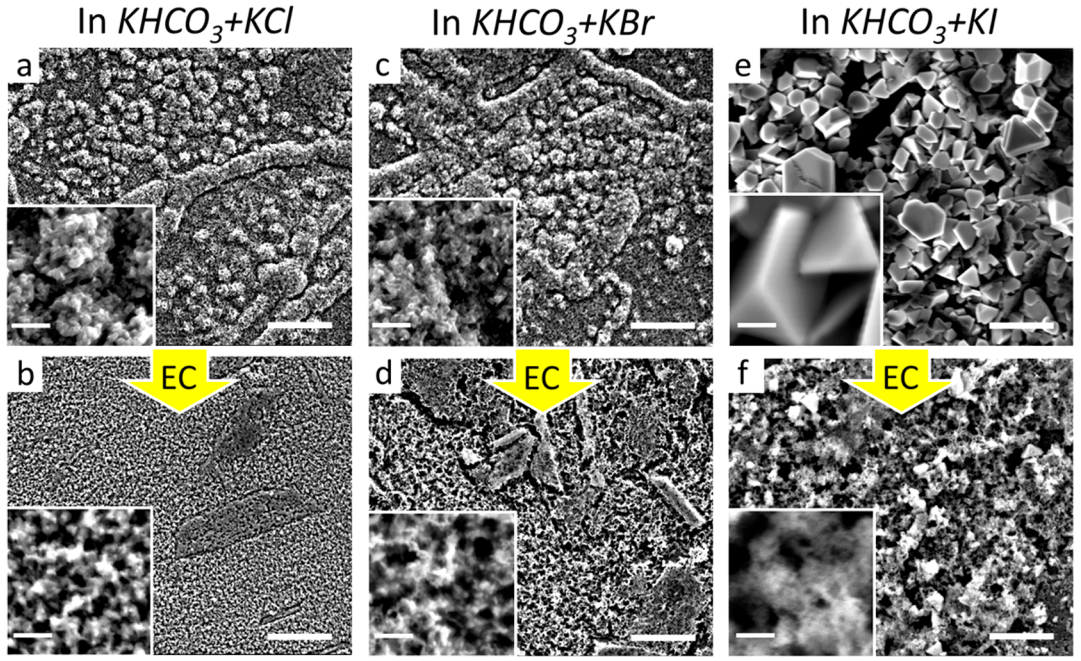

Figure 1. SEM images of O_2-plasma-treated Cu foils acquired before (a,c,e) and after (b,d,f) the CO_2 electroreduction. The images in the top row were acquired after sample immersion in the following electrolytes for 30 min: (a) 0.1 M $KHCO_3$ + 0.3 M KCl, (c) 0.1 M $KHCO_3$ + 0.3 M KBr, and (e) 0.1 M $KHCO_3$ + 0.3 M KI. Those in the bottom row were acquired after 1 h of CO_2 electroreduction at −1.0 V vs RHE in the corresponding electrolytes. The scale bars in the main images and inserts are 5 μm and 500 nm, respectively.

foil with a low-pressure O_2 plasma.[18] Figure 1 shows typical SEM images of the Cu foils treated with O_2 plasma and subsequently immersed in $KHCO_3$ + KX (X = Cl, Br, I) for 30 min before (Figure 1a,c,e) and after (Figure 1b,d,f) 1 h of CO_2 electroreduction at ca. −1.0 V vs RHE. SEM data from a reference sample consisting of a plasma-oxidized Cu foil measured before electrolyte exposure, after 30 min in $KHCO_3$, and after 1 h of CO_2 electroreduction are included in Figure S1 in the Supporting Information. The electropolished Cu foil was severely oxidized by the O_2-plasma treatment, forming a highly roughened surface with obvious pore structures (Figure S1a). A high oxygen content (~41%, atomic percentage) was confirmed by energy dispersive X-ray spectroscopy (EDX) analysis (Table S1 in the Supporting Information), corresponding to a mixture of CuO and Cu_2O species in surface and near-surface regions (probing depth of ~300 nm at 10 keV). Prior to the electrochemical measurements, the electrolyte was saturated by bubbling CO_2 for 30 min to remove oxygen in the solution. No drastic differences were observed in the Cu surface morphology when the oxidized Cu foils were introduced in the $KHCO_3$ (Figure S1b), $KHCO_3$ + KCl (Figure 1a), and $KHCO_3$ + KBr (Figure 1c) solutions.

Interestingly, when the Cu foil was introduced in the electrolyte containing I^- for 30 min, some well-defined Cu crystals were formed (Figure 1e), and EDX analysis (Table S1 in the Supporting Information) showed that most of the oxygen in the oxidized Cu foil was replaced by iodine (~41% O in the as-prepared sample versus ~17% O and ~35% I in the sample previously submerged in $KHCO_3$ + KI). This spontaneous and selective nanostructuring of the oxidized Cu foil in KI solution even at open circuit potential is caused by the strong affinity between Cu^+ and I^-.[52−54] When the reaction was carried out in pure $KHCO_3$, the morphology did not reveal any significant change in comparison with the as-prepared sample (Figure S1c in the Supporting Information), while the majority of the oxygen signal was depleted during the reaction (from ~41% to ~4% O, Table S1). On the other hand, obvious differences in the morphology were observed after the reaction when it was conducted in the presence of halides (Figure 1b,d,f). The preformed Cu crystals and high content of iodine were strongly depleted during the reaction. It should be mentioned that the samples were washed thoroughly with water and transferred immediately to the SEM chamber after the reaction. Nevertheless, the addition of halides led to further nanostructuring under the reaction conditions of the already roughened preoxidized Cu surface, producing a large number of small pores, especially in the case of I^-. This is similar to other halide-induced morphological changes previously reported for pure metallic surfaces.[55] In spite of the originally identical oxidized state and brief exposure to air before SEM, the samples after the reaction in $KHCO_3$ with addition of either Br^- or I^- showed higher oxygen content in comparison to those after the reaction in pure $KHCO_3$ and in the presence of Cl^- (Table S1). Within the error of the EDX measurements, no halide residues could be detected on the surface of the samples after the reaction in the halide-containing electrolytes (Table S1).

In order to confirm the effect of electrolyte-driven nanostructuring on the CO_2 electroreduction, we conducted quasi in situ XPS studies on the O_2-plasma-treated Cu foil, as well as an electropolished Cu foil for comparison. CO_2 electroreduction was carried out on these samples for 1 h in different CO_2-saturated electrolytes at −1.0 V vs RHE in a commercial cell (SPECS GmbH) attached to an UHV system (Figure S2 in the Supporting Information).[19] Subsequently, the samples were transferred in UHV to an adjacent chamber where an XPS analyzer was available. The deconvolution of Cu Auger spectra (Figure 2 and Figure S3 and Table S2 in the Supporting Information) is more reliable for the determination of the content of Cu^+ species in comparison to that of the O 1s (Figure S4 in the Supporting Information) and Cu 2p spectra

DOI: 10.1021/acscatal.7b01416
ACS Catal. 2017, 7, 5112−5120

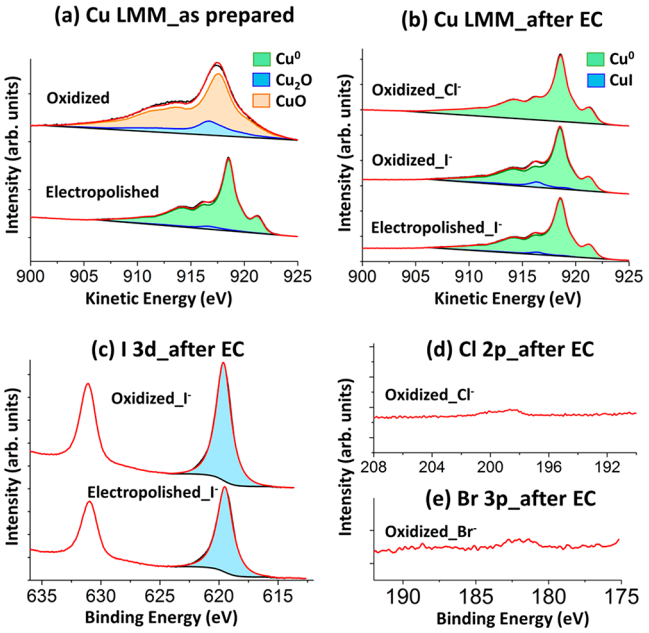

Figure 2. Quasi in situ Cu Auger LMM XPS spectra of the fresh O_2-plasma-oxidized and an electropolished Cu foil (a) and the same samples after 1 h of CO_2 electroreduction at −1.0 V vs RHE in 0.1 M $KHCO_3$ + 0.3 M KI, and 0.1 M $KHCO_3$ + 0.3 M KCl (b). Core level signals from I 3d (c), Cl 2p (d), and Br 3p (e) acquired after reaction in the corresponding electrolytes are also shown. The data in (c) correspond to the final state of the oxidized and electropolished Cu foil samples after reaction in 0.1 M $KHCO_3$ + 0.3 M KI, in situ sample wash, and in situ XPS transfer. The data in (c) and (d) were acquired on the plasma-oxidized Cu foil after reaction in 0.1 M $KHCO_3$ + 0.3 M KCl and 0.1 M $KHCO_3$ + 0.3 M KBr, respectively.

(Figure S5 in the Supporting Information). For the deconvolution of the Auger spectra, the envelopes of Auger spectra of reference samples (see the Experimental Section) were used. Figure 2a shows the Cu Auger LMM spectra for the as-prepared plasma-oxidized and electropolished Cu foils. The XPS spectra showed that the surface of the fresh plasma-oxidized Cu foil was also composed of CuO (85%, atomic percentage) and Cu_2O (15%), consistent with EDX analysis of the bulk. A small amount of Cu_2O (5%, 95% metallic Cu) was visible on the fresh electropolished Cu foil due to the fast oxidation of metallic Cu during the transfer in air to the XPS chamber. After 1 h of the reaction in 0.1 M $KHCO_3$ + 0.3 M KI, the O_2-plasma-oxidized Cu foil was mostly reduced with ~91% metallic Cu and ~9% Cu^+ species (Figure 2b). By carefully analyzing the O 1s (Figure S4) and I 3d (Figure 2c) data, we confirmed that most of the Cu^+ species detected after the reaction exist in the form of CuI. A small CuI signal was also observed on the electropolished Cu foil after the reaction in 0.1 M $KHCO_3$ + 0.3 M KI, which is likely stabilized due to the initial presence of Cu_2O in this sample due to the sample transfer in air to the in situ EC chamber before reaction. Therefore, the presence of I^- in the electrolyte results in the stabilization of the Cu^+ species on the sample surface in the form of CuI (Table S3 in the Supporting Information). In the case of Cl^- and Br^-, no Cu^+ species were observed after the reaction (Figure 2b), and only trace amounts of Cl (Figure 2d) and Br (Figure 2e) were present.

The effect of halides on the catalytic performance of O_2-plasma-oxidized Cu foils was studied by performing chronoamperometry measurements in 0.1 M $KHCO_3$ or 0.1 M $KHCO_3$ + 0.3 M KX (X = Cl, Br, I). In this study, 0.1 M $KHCO_3$ was used as a reference and a buffer to avoid significant changes in the pH which could alter the reaction pathway for hydrocarbon formation.[36,37,45] The O_2-plasma-oxidized Cu foils in all electrolytes show much higher current densities (Figure 3a and Figure S6a in the Supporting Information) in comparison to the electropolished foil in pure $KHCO_3$, mainly attributed to the presence of Cu^+ species and subsurface oxygen during the reaction.[18,19] The presence of halides in the electrolyte strongly affects the catalytic activity of oxidized Cu foils. The addition of halides increased the current densities, following the trend no halide < Cl^- < Br^- < I^-.

Figure 3b and Figure S6b in the Supporting Information compares the total FEs for C_2−C_3 products of the mainly metallic electropolished Cu foil in $KHCO_3$ to that of the oxidized samples in the same pure electrolyte, as well as in those containing halides. A drastic increase in the C_2−C_3 production (up to ~65% FE) was observed for all preoxidized samples in comparison to the electropolished foil (~23%) at −1.0 V vs RHE. The former total C_2−C_3 FE is higher than that previously reported for Cu-based catalysts (Table S4 in the Supporting Information). Figure 4 and Figure S7 in the Supporting Information show the potential-dependent individual production rates of the different products, and the corresponding partial current densities and FEs are presented in Figures S8 and S9 in the Supporting Information, respectively. In all electrolytes, the O_2-plasma-oxidized Cu foils showed a remarkable increased ethylene production rate in comparison to the electropolished foil (Figure 4a), while

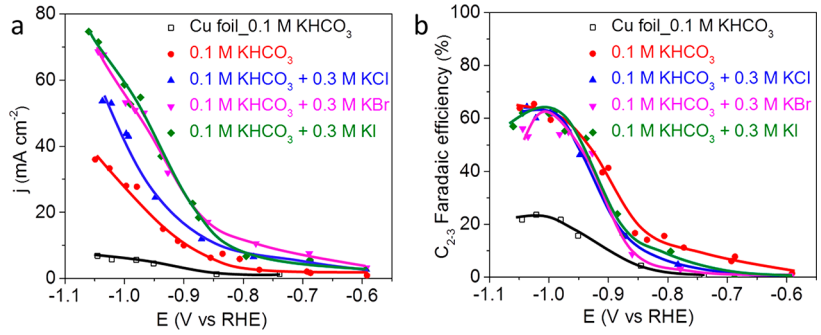

Figure 3. (a) Current density and (b) total Faradaic efficiency of C_2−C_3 products as a function of applied potential for O_2-plasma-treated Cu foils in different electrolytes, as well as for an electropolished Cu foil (open squares) in pure $KHCO_3$ solution after 1 h of CO_2 electroreduction. Solid lines are guides for the eye. Error bars are shown in Figure S6 in the Supporting Information.

DOI: 10.1021/acscatal.7b01416
ACS Catal. 2017, 7, 5112−5120

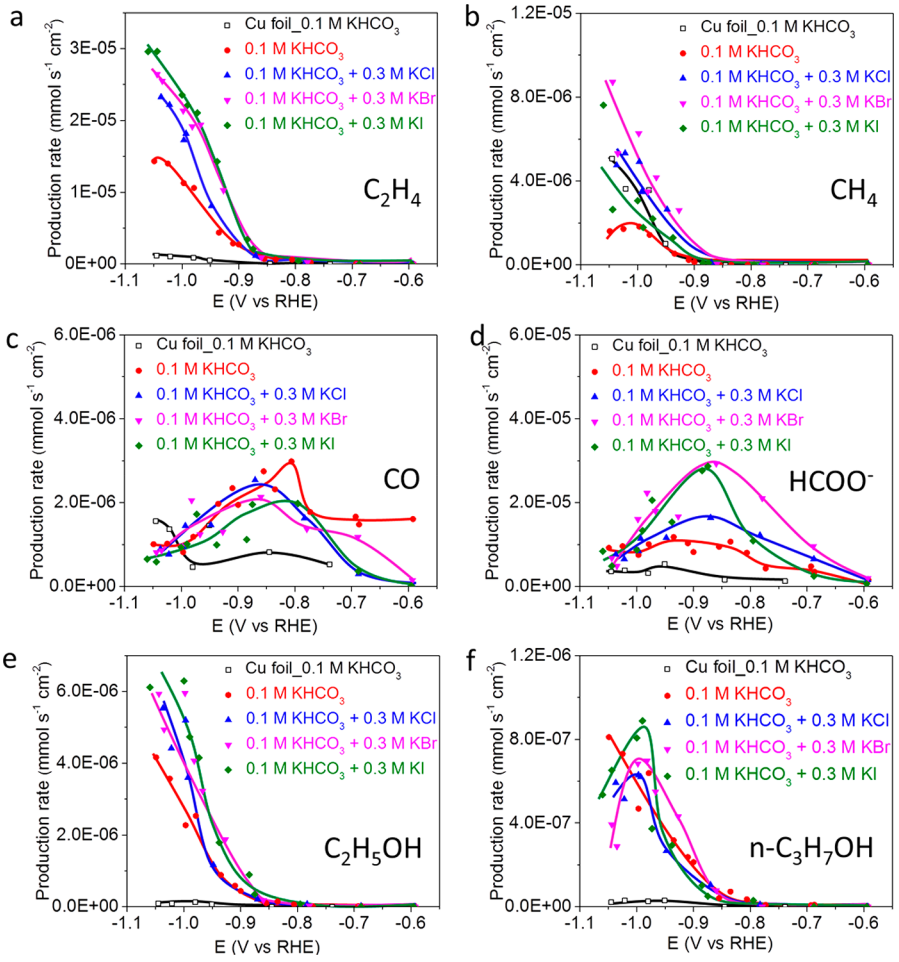

Figure 4. Production rates of (a) C_2H_4, (b) CH_4, (c) CO, (d) $HCOO^-$, (e) C_2H_5OH, and (f) *n*-C_3H_7OH as a function of applied potential for O_2-plasma-treated Cu foils in different electrolytes, as well as for an electropolished metallic Cu foil (open squares) in pure $KHCO_3$ solution after 1 h of CO_2 electroreduction. Solid lines are guides for the eye.

methane production rates were similar (Figure 4b), resulting in the high ethylene FE (Figure S9a) and very low methane FE (Figure S9b). Similar trends were also observed on ethanol (Figure 4e and Figure S9e) and *n*-propanol (Figure 4f and Figure S9f) formation. Figure S10 in the Supporting Information shows the potentials required to achieve ∼50% of the highest production rate in different electrolytes at −1.0 V vs RHE for ethylene and ethanol formation. The addition of halides positively shifted the potentials (lower negative value) for ethylene and ethanol formation in comparison with that in pure $KHCO_3$. These potentials followed the same trend (no halide < Cl^- < Br^- < I^-) with the current densities, suggesting the most significant promoting effect of I^- on C_2−C_3 product formation. CO formation (Figure 4c and Figure S9c) was suppressed at less negative potentials (−0.6 to −0.8 V vs RHE) in the presence of halides, while formate formation (Figure 4d and Figure S9d) was facilitated at intermediate potentials (−0.7 to −0.95 V vs RHE). The hydrogen evolution reaction was also facilitated at less negative potentials in the presence of halides (Figures S7c and S9i). At more negative potentials (around −1.0 V vs RHE), the presence of I^- slightly suppressed the formation of methane and CO in comparison to Cl^- and Br^- (Figure 4b,c), leading to a higher FE ratio of $(C_2 + C_3)/C_1$ (Figure S11 in the Supporting Information). Therefore, I^- induced more selective CO_2 reduction to C_2−C_3 products. Trace amounts (<1% FE) of ethane (Figures S7a and S9g) and acetate (Figures S7b and S9h) were also produced. Therefore, the presence of halides in electrolytes enhances the activity of O_2-plasma-treated Cu foils, without sacrificing their intrinsically high C_2−C_3 product selectivity.

The catalytic performance enhancement could be attributed to an increased roughness[17] induced by in situ halide nanostructuring during the reaction (Figure 1), defects,[12−14] and strain effects[32,33,56] and/or increased subsurface/surface oxygen content retained during the reaction.[18,19,57,58] Roughness factors were determined by measuring the double-layer capacitance of each of the halide-modified surfaces after 1 h of CO_2 electroreduction and subsequent sample wash in water (Table S5 in the Supporting Information). The obtained capacitance values were normalized by that of an electropolished Cu foil (Figure S12 in the Supporting Information).[19] Consistent with the fact that I^- induced the most significant morphological change (Figure 1e), the sample after the reaction in the presence of I^- shows the highest roughness factor, ∼1.5 times higher than that of the sample exposed to Br^- during the reaction. However, the above two samples (with similar oxygen content, Table S1 in the Supporting Information) have similar current densities; thus, the roughness effect cannot by itself explain the halide-induced enhancement in current density (Figure 3a). The sample after the reaction in the presence of Br^- has similar roughness but higher oxygen content (6.1 atom % versus 3.5 atom % from EDX analysis) in comparison to that

DOI: 10.1021/acscatal.7b01416
ACS Catal. 2017, 7, 5112−5120

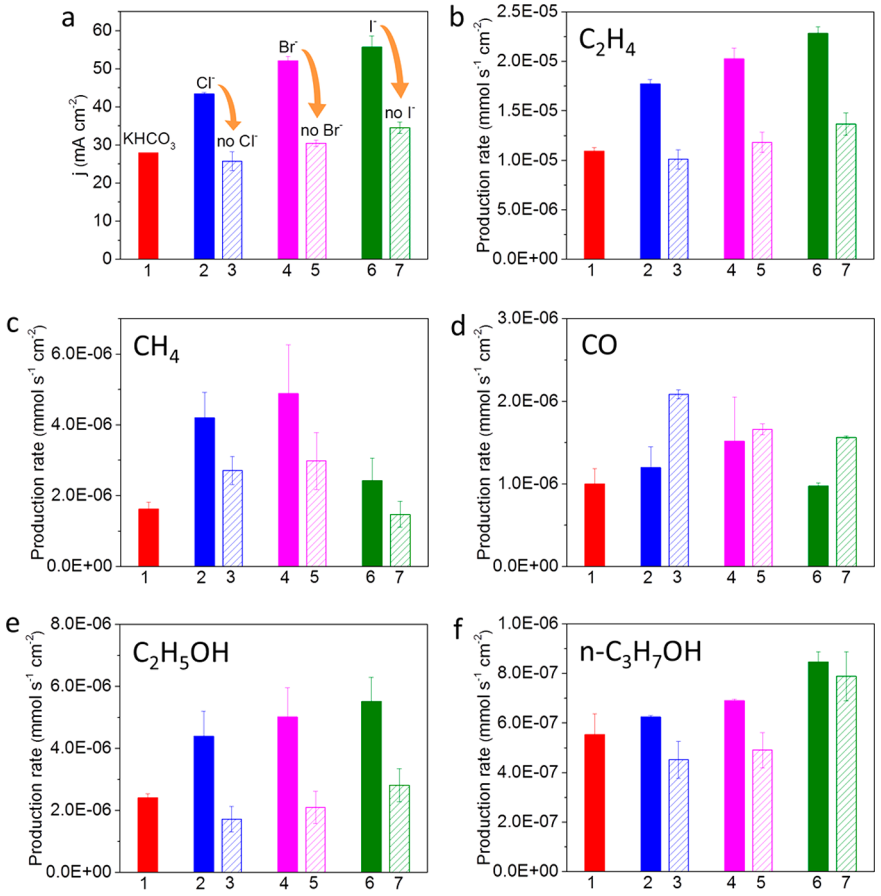

Figure 5. Current density (a) and production rate of (b) C_2H_4, (c) CH_4, (d) CO, (e) C_2H_5OH, and (f) *n*-C_3H_7OH on the O_2-plasma-treated Cu foils after 1 h of CO_2 electroreduction in different electrolytes at −1.0 V vs RHE: (1) 0.1 M $KHCO_3$; (2) 0.1 M $KHCO_3$ + 0.3 M KCl; (3) same sample as (2) but measured in 0.1 M $KHCO_3$ without KCl; (4) 0.1 M $KHCO_3$ + 0.3 M KBr; (5) same sample as (4) but measured in 0.1 M $KHCO_3$ without KBr; (6) 0.1 M $KHCO_3$ + 0.3 M KI; (7) same sample as (6) but measured in 0.1 M $KHCO_3$ without KI.

after the reaction in the presence of Cl^-, and its current density is ∼1.2 times higher than the latter (Figure 3a), suggesting the possible role of oxygen species in enhancing the activity. It should be noted that the significant difference in ethylene/methane selectivity among our reference sample here, a halide-free O_2-plasma-activated Cu foil, and a polished Cu foil[45] has been previously attributed to the presence of subsurface oxygen and Cu^+ species bound to oxygen,[18,19,57,58] as well as to an increased surface roughness[17] and to special defect sites available in oxide-derived Cu.[12−14] Nevertheless, apart from varying the roughness and oxygen content of the Cu surface, halides could also have a chemical effect on CO_2 electroreduction due to their strong adsorption on Cu surfaces.[46]

In order to confirm the chemical effect and better decouple it from a simple halide-induced surface roughening, we ran the CO_2 electroreduction in pure $KHCO_3$ on those *restructured* samples after 1 h of the reaction in the presence of halides at around −1.0 V vs RHE. After the first measurements in 0.1 M $KHCO_3$ + 0.3 M KX, these samples were washed thoroughly to remove residual halide ions (which are not available as CuI species, as suggested by XPS in Figure 2) and then transferred to pure 0.1 M $KHCO_3$. The catalytic performances in both cases are shown in Figure 5 and Figures S13 and S14 in the Supporting Information. Obvious differences were observed in the current densities and production rates, when as starting materials either fresh O_2-plasma-treated samples in an electrolyte containing the halides, versus already halide pre-*restructured* samples measured in a halide-free electrolyte ($KHCO_3$) were used. In particular, better activity was observed when the halides were present in the electrolyte, demonstrating a chemical effect on the reaction.

Furthermore, the catalytic activity of the *restructured* samples, when they were measured in the absence of halides, was not only much lower than that of the fresh samples but was similar to or only slightly higher than that of the fresh samples in pure $KHCO_3$. The latter suggests that the chemical effect of the halides plays a much more important role in the improved catalytic performance in comparison to the roughness and oxygen content, since both were higher on the halide-treated samples. The fact that the I^--*restructured* sample showed slightly higher activity than the Br^--*restructured* sample in pure $KHCO_3$ also confirmed the minor effect of roughness.

Halide ions are usually considered to participate in or influence electrochemical reactions due to the nature of their strong adsorption on the surface of electrodes. A density functional theory study by Janik et al.[46] indicated that the specific adsorption of aqueous Cl^-, Br^-, and I^- on Cu (111), (100), and (211) surfaces can occur at potentials where CO_2 reduction is usually carried out; therefore, these halides probably affect the reaction. The adsorption is increasingly favorable in the order of Cl^- < Br^- < I^- on all Cu facets and is most favorable on Cu (100),[46] which is considered the favorable facet for C−C coupling both thermodynamically and kinetically.[58−62] In order to clarify the chemical effect of

DOI: 10.1021/acscatal.7b01416
ACS Catal. 2017, 7, 5112−5120

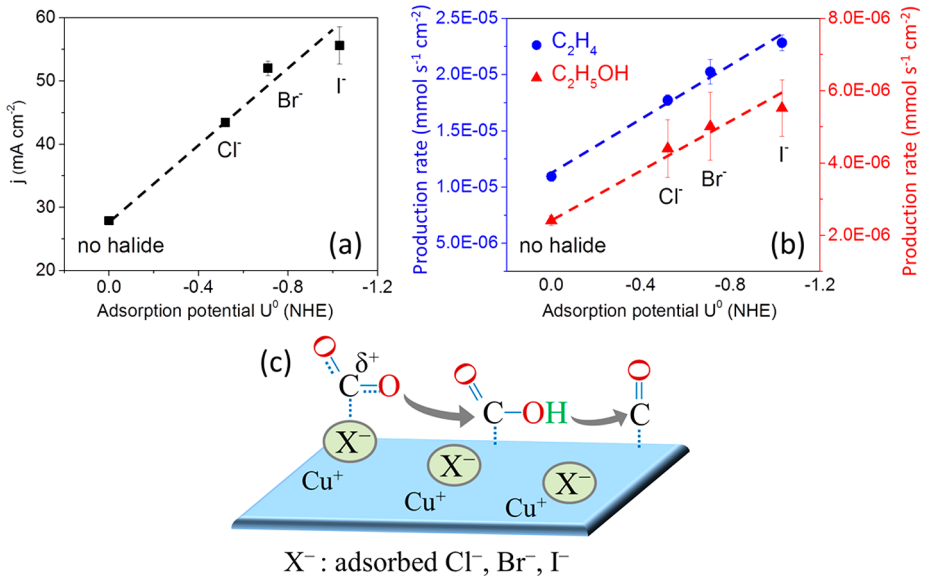

Figure 6. Correlations between current density (a) and production rates of ethylene and ethanol (b) in different electrolytes at −1.0 V vs RHE and theoretically predicted halide adsorption potential on Cu (100) extracted from ref 46. (c) Illustration of how adsorbed halides facilitate CO_2 adsorption and stabilize the carboxyl intermediate.

halides, we link the halide-enhanced catalytic performance to their theoretical results. Figure 6a,b quantitatively describes the correlation between catalytic performance and the chemical effect of the halides on CO_2 electroreduction. The current density shows a nearly linear relationship with the adsorption energy of halides on the Cu (100) facet (Figure 6a). Similar trends are also observed on ethylene and ethanol production rates (Figure 6b). Therefore, although electrolyte-driven nanostructuring induced obvious morphology changes before and during the reaction, especially in the case of I^-, the enhanced catalytic activity trend (no halide < Cl^- < Br^- < I^-) was mainly attributed to the increased halide adsorption energy.

A previous study[45] on the halide effect on an electropolished Cu foil showed the increased CO selectivity in the presence of Cl^- and Br^- and the increased methane selectivity in the presence of I^-. In contrast, on our oxidized Cu foils the activities were significantly enhanced in the presence of all halides without sacrificing their intrinsically high C_2−C_3 product selectivity, demonstrating a promoting effect of halide on CO_2 electroreduction. The intrinsically higher activity and selectivity of our oxidized Cu catalyst over electropolished Cu foil is mainly attributed to the presence of subsurface oxygen and Cu^+ species during the reaction.[18,19] Although a Cu^+ species after 1 h of the reaction was only observed by XPS on the sample in KI solution, there could be a gradient in the Cu^+ content inside the oxidized Cu foil, with lower Cu^+ content near the surface. In comparison with the Cu single crystal, a roughened Cu surface contains significantly more low-coordination sites, such as steps, corners, and defects,[63] which would further increase the adsorption of halides. Although only iodine ions can be found by XPS in significant amounts after the reaction, it should be noted that XPS measurements were done after thoroughly washing the sample with water after the reaction in situ (no air exposure before the transfer to the XPS system), which probably removed the other more weakly adsorbed halides. The Cu^+ species, bound to subsurface oxygen, could play a vital role in enhancing the adsorption of halides by a strong Coulomb interaction. Thus, a layer with high coverage of halides may be formed on the Cu surface during the reaction.

Given that the addition of halides does not significantly change the selectivity but only increases the production rates of most products at around −1.0 V vs RHE, the effect of halides on CO_2 electroreduction may affect a common step for the formation of all products. Possible reaction pathways of CO_2 electroreduction on Cu have been discussed comprehensively among others by Koper et al.[7] Adsorbed CO is first formed via the carboxyl (*COOH) intermediate and further reduced by protons and electrons to CO and then to hydrocarbons and alcohols. The formation of CO is a common step for the formation of all hydrocarbon and alcohols. The formation of *COOH is considered as the rate-determining step for CO production. Therefore, the formation of *COOH through a concerted proton−electron transfer to CO_2 is probably facilitated by the adsorbed halides with high coverage on the Cu surface. Here, we proposed a mechanism for the effect of halides on CO_2 electroreduction, as shown in Figure 6c. The halides specifically adsorbed on the Cu surface donate their partial charge to the carbon atom in the CO_2 molecule, which forms a covalent X^-−C bond and causes the structural transformation of CO_2 from the linear form to the bent $CO_2^{\delta-}$ species.[44] The bent $CO_2^{\delta-}$ species adsorbed on the surface is further converted to *COOH via a concerted proton−electron transfer.[7] Therefore, the specific adsorbed halides, on the Cu catalyst with the subsurface oxygen and Cu^+ species, facilitate the adsorption of CO_2 and stabilize the key *COOH intermediate. In comparison with the thermodynamically less favored CO_2 adsorption on the Cu surface,[64] the halide-assisted CO_2 adsorption is greatly facilitated by the high electron density of halide ions. This enhancement effect depends on the specific adsorption ability of halide ions (I^- > Br^- > Cl^-), which explains very well the CO_2 electroreduction performance trend of our oxidized Cu foil (no halide < Cl^- < Br^- < I^-).

4. CONCLUSIONS

In summary, we studied the effect of halides on CO_2 electroreduction by the addition of halides to the $KHCO_3$ electrolyte. Halide ions can induce significant nanostructuring

DOI: 10.1021/acscatal.7b01416
ACS Catal. 2017, 7, 5112−5120

of the oxidized Cu surface, even at open circuit potential, as is the case for I^-, which leads to the formation of well-defined Cu nanocrystals. Furthermore, the presence of halides was found to lower the overpotential and to increase the CO_2 electroreduction rate on plasma-activated Cu catalysts without losing their intrinsically high C_2-C_3 selectivity. This enhancement in catalytic performance is mainly attributed to the specific adsorption of halides with a higher coverage on our preoxidized Cu surface during the reaction, which on the basis of previous theoretical work may donate partial charge from halide ions to the CO_2 molecule. The latter is thought to facilitate the adsorption of CO_2 and the stabilization of the carboxyl intermediate via the transfer of charge from the Cu surface to CO_2. This work provides new insights into the importance of electrolyte-driven surface restructuring and electronic modification in the design of electrocatalysts.

■ ASSOCIATED CONTENT

Supporting Information

The Supporting Information is available free of charge on the ACS Publications website at DOI: 10.1021/acscatal.7b01416.

Calculations of FE and production rate, additional SEM images, EDX analysis, XPS data, additional analysis of the electrochemical data, and roughness factor measurements (PDF)

■ AUTHOR INFORMATION

Corresponding Author

*E-mail for B.R.C.: Beatriz.Roldan@rub.de.

ORCID

Dunfeng Gao: 0000-0002-2472-7349

Beatriz Roldan Cuenya: 0000-0002-8025-307X

Notes

The authors declare no competing financial interest.

■ ACKNOWLEDGMENTS

This work was funded by the Cluster of Excellence RESOLV at RUB (EXC 1069) funded by the Deutsche Forschungsgemeinschaft and the German Federal Ministry of Education and Research (Bundesministerium für Bildung und Forschung, BMBF) under grant #03SF0523C-'CO2EKAT.' Partial financial support from the U.S. National Science Foundation (NSF-Chemistry 1213182) is also greatly appreciated.

■ REFERENCES

(1) Montoya, J. H.; Seitz, L. C.; Chakthranont, P.; Vojvodic, A.; Jaramillo, T. F.; Nørskov, J. K. *Nat. Mater.* **2017**, *16*, 70−81.

(2) Martin, A. J.; Larrazabal, G. O.; Perez-Ramirez, J. *Green Chem.* **2015**, *17*, 5114−5130.

(3) Whipple, D. T.; Kenis, P. J. A. *J. Phys. Chem. Lett.* **2010**, *1*, 3451−3458.

(4) Hori, Y. In *Modern Aspects of Electrochemistry*; Vayenas, C. G., White, R. E., Gamboa-Aldeco, M. E., Eds.; Springer: New York, 2008; pp 89−189.

(5) Mistry, H.; Varela, A. S.; Kuhl, S.; Strasser, P.; Roldan Cuenya, B. *Nat. Rev. Mater.* **2016**, *1*, 16009.

(6) Gao, D. F.; Cai, F.; Wang, G. X.; Bao, X. H. *Curr. Opin. Green Sustainable Chem.* **2017**, *3*, 39−44.

(7) Kortlever, R.; Shen, J.; Schouten, K. J. P.; Calle-Vallejo, F.; Koper, M. T. M. *J. Phys. Chem. Lett.* **2015**, *6*, 4073−4082.

(8) Peterson, A. A.; Abild-Pedersen, F.; Studt, F.; Rossmeisl, J.; Nørskov, J. K. *Energy Environ. Sci.* **2010**, *3*, 1311−1315.

(9) Reske, R.; Mistry, H.; Behafarid, F.; Roldan Cuenya, B.; Strasser, P. *J. Am. Chem. Soc.* **2014**, *136*, 6978−6986.

(10) Mistry, H.; Behafarid, F.; Reske, R.; Varela, A. S.; Strasser, P.; Roldan Cuenya, B. *ACS Catal.* **2016**, *6*, 1075−1080.

(11) Mistry, H.; Reske, R.; Strasser, P.; Roldan Cuenya, B. *Catal. Today* **2017**, *288*, 30.

(12) Li, C. W.; Ciston, J.; Kanan, M. W. *Nature* **2014**, *508*, 504−507.

(13) Li, C. W.; Kanan, M. W. *J. Am. Chem. Soc.* **2012**, *134*, 7231−7234.

(14) Verdaguer-Casadevall, A.; Li, C. W.; Johansson, T. P.; Scott, S. B.; McKeown, J. T.; Kumar, M.; Stephens, I. E. L.; Kanan, M. W.; Chorkendorff, I. *J. Am. Chem. Soc.* **2015**, *137*, 9808−9811.

(15) Roberts, F. S.; Kuhl, K. P.; Nilsson, A. *Angew. Chem., Int. Ed.* **2015**, *54*, 5179−5182.

(16) Loiudice, A.; Lobaccaro, P.; Kamali, E. A.; Thao, T.; Huang, B. H.; Ager, J. W.; Buonsanti, R. *Angew. Chem., Int. Ed.* **2016**, *55*, 5789−5792.

(17) Kas, R.; Kortlever, R.; Yilmaz, H.; Koper, M. T. M.; Mul, G. *ChemElectroChem* **2015**, *2*, 354−358.

(18) Mistry, H.; Varela, A. S.; Bonifacio, C. S.; Zegkinoglou, I.; Sinev, I.; Choi, Y. W.; Kisslinger, K.; Stach, E. A.; Yang, J. C.; Strasser, P.; Roldan Cuenya, B. *Nat. Commun.* **2016**, *7*, 12123.

(19) Gao, D. F.; Zegkinoglou, I.; Divins, N. J.; Scholten, F.; Sinev, I.; Grosse, P.; Roldan Cuenya, B. *ACS Nano* **2017**, *11*, 4825−4831.

(20) Lee, S.; Kim, D.; Lee, J. *Angew. Chem., Int. Ed.* **2015**, *54*, 14701−14705.

(21) Reller, C.; Krause, R.; Volkova, E.; Schmid, B.; Neubauer, S.; Rucki, A.; Schuster, M.; Schmid, G. *Adv. Energy Mater.* **2017**, *7*, 1602114.

(22) Engelbrecht, A.; Hammerle, M.; Moos, R.; Fleischer, M.; Schmid, G. *Electrochim. Acta* **2017**, *224*, 642−648.

(23) Eilert, A.; Cavalca, F.; Roberts, F. S.; Osterwalder, J.; Liu, C.; Favaro, M.; Crumlin, E. J.; Ogasawara, H.; Friebel, D.; Pettersson, L. G.; Nilsson, A. *J. Phys. Chem. Lett.* **2017**, *8*, 285−290.

(24) Kattel, S.; Yan, B. H.; Yang, Y. X.; Chen, J. G. G.; Liu, P. *J. Am. Chem. Soc.* **2016**, *138*, 12440−12450.

(25) Eren, B.; Weatherup, R. S.; Liakakos, N.; Somorjai, G. A.; Salmeron, M. *J. Am. Chem. Soc.* **2016**, *138*, 8207−8211.

(26) Ren, D.; Deng, Y. L.; Handoko, A. D.; Chen, C. S.; Malkhandi, S.; Yeo, B. S. *ACS Catal.* **2015**, *5*, 2814−2821.

(27) Rosen, B. A.; Salehi-Khojin, A.; Thorson, M. R.; Zhu, W.; Whipple, D. T.; Kenis, P. J. A.; Masel, R. I. *Science* **2011**, *334*, 643−644.

(28) Asadi, M.; Kim, K.; Liu, C.; Addepalli, A. V.; Abbasi, P.; Yasaei, P.; Phillips, P.; Behranginia, A.; Cerrato, J. M.; Haasch, R.; Zapol, P.; Kumar, B.; Klie, R. F.; Abiade, J.; Curtiss, L. A.; Salehi-Khojin, A. *Science* **2016**, *353*, 467−470.

(29) Asadi, M.; Kumar, B.; Behranginia, A.; Rosen, B. A.; Baskin, A.; Repnin, N.; Pisasale, D.; Phillips, P.; Zhu, W.; Haasch, R.; Klie, R. F.; Kral, P.; Abiade, J.; Salehi-Khojin, A. *Nat. Commun.* **2014**, *5*, 4470.

(30) Neubauer, S. S.; Krause, R. K.; Schmid, B.; Guldi, D. M.; Schmid, G. *Adv. Energy Mater.* **2016**, *6*, 1502231.

(31) Liu, M.; Pang, Y. J.; Zhang, B.; De Luna, P.; Voznyy, O.; Xu, J. X.; Zheng, X. L.; Dinh, C. T.; Fan, F. J.; Cao, C. H.; de Arquer, F. P. G.; Safaei, T. S.; Mepham, A.; Klinkova, A.; Kumacheva, E.; Filleter, T.; Sinton, D.; Kelley, S. O.; Sargent, E. H. *Nature* **2016**, *537*, 382−386.

(32) Chen, L. D.; Urushihara, M.; Chan, K. R.; Nørskov, J. K. *ACS Catal.* **2016**, *6*, 7133−7139.

(33) Sandberg, R. B.; Montoya, J. H.; Chan, K.; Nørskov, J. K. *Surf. Sci.* **2016**, *654*, 56−62.

(34) Murata, A.; Hori, Y. *Bull. Chem. Soc. Jpn.* **1991**, *64*, 123−127.

(35) Singh, M. R.; Kwon, Y.; Lum, Y.; Ager, J. W.; Bell, A. T. *J. Am. Chem. Soc.* **2016**, *138*, 13006−13012.

(36) Schouten, K. J. P.; Gallent, E. P.; Koper, M. T. M. *J. Electroanal. Chem.* **2014**, *716*, 53−57.

(37) Hori, Y.; Takahashi, R.; Yoshinami, Y.; Murata, A. *J. Phys. Chem. B* **1997**, *101*, 7075−7081.

(38) Kim, B.; Ma, S.; Molly Jhong, H.-R.; Kenis, P. J. A. *Electrochim. Acta* **2015**, *166*, 271−276.

DOI: 10.1021/acscatal.7b01416
ACS Catal. 2017, 7, 5112−5120

(39) Gao, D. F.; Wang, J.; Wu, H. H.; Jiang, X. L.; Miao, S.; Wang, G. X.; Bao, X. H. *Electrochem. Commun.* **2015**, *55*, 1−5.
(40) Hori, Y.; Murata, A.; Takahashi, R. *J. Chem. Soc., Faraday Trans. 1* **1989**, *85*, 2309−2326.
(41) Dunwell, M.; Lu, Q.; Heyes, J. M.; Rosen, J.; Chen, J. G.; Yan, Y.; Jiao, F.; Xu, B. *J. Am. Chem. Soc.* **2017**, *139*, 3774−3783.
(42) Tripkovic, D. V.; Strmcnik, D.; van der Vliet, D.; Stamenkovic, V.; Markovic, N. M. *Faraday Discuss.* **2009**, *140*, 25−40.
(43) Ogura, K.; Ferrell, J. R.; Cugini, A. V.; Smotkin, E. S.; Salazar-Villalpando, M. D. *Electrochim. Acta* **2010**, *56*, 381−386.
(44) Ogura, K. *J. CO2 Util.* **2013**, *1*, 43−49.
(45) Varela, A. S.; Ju, W.; Reier, T.; Strasser, P. *ACS Catal.* **2016**, *6*, 2136−2144.
(46) McCrum, I. T.; Akhade, S. A.; Janik, M. J. *Electrochim. Acta* **2015**, *173*, 302−309.
(47) Akhade, S. A.; McCrum, I. T.; Janik, M. J. *J. Electrochem. Soc.* **2016**, *163*, F477−F484.
(48) Verma, S.; Xu, L.; Ma, S. C.; Masel, R. I.; Kenis, P. J. A. *Phys. Chem. Chem. Phys.* **2016**, *18*, 7075−7084.
(49) Verma, S.; Kim, B.; Jhong, H.; Ma, S. C.; Kenis, P. J. A. *ChemSusChem* **2016**, *9*, 1972−1979.
(50) Biesinger, M. C.; Lau, L. W. M.; Gerson, A. R.; Smart, R. S. C. *Appl. Surf. Sci.* **2010**, *257*, 887−898.
(51) Xiang, C. X.; Kimball, G. M.; Grimm, R. L.; Brunschwig, B. S.; Atwater, H. A.; Lewis, N. S. *Energy Environ. Sci.* **2011**, *4*, 1311−1318.
(52) Lefevre, G.; Walcarius, A.; Ehrhardt, J. J.; Bessiere, J. *Langmuir* **2000**, *16*, 4519−4527.
(53) Hsiao, G. S.; Anderson, M. G.; Gorer, S.; Harris, D.; Penner, R. M. *J. Am. Chem. Soc.* **1997**, *119*, 1439−1448.
(54) Ng, C. H. B.; Fan, W. Y. *J. Phys. Chem. B* **2006**, *110*, 20801−20807.
(55) Hsieh, Y. C.; Senanayake, S. D.; Zhang, Y.; Xu, W. Q.; Polyansky, D. E. *ACS Catal.* **2015**, *5*, 5349−5356.
(56) Huang, H. W.; Jia, H. H.; Liu, Z.; Gao, P. F.; Zhao, J. T.; Luo, Z. L.; Yang, J. L.; Zeng, J. *Angew. Chem., Int. Ed.* **2017**, *56*, 3594−3598.
(57) Favaro, M.; Xiao, H.; Cheng, T.; Goddard, W. A.; Yano, J.; Crumlin, E. J. *Proc. Natl. Acad. Sci. U. S. A.* **2017**, 201701405.
(58) Xiao, H.; Goddard, W. A.; Cheng, T.; Liu, Y. Y. *Proc. Natl. Acad. Sci. U. S. A.* **2017**, 201702405.
(59) Cheng, T.; Xiao, H.; Goddard, W. A. *Proc. Natl. Acad. Sci. U. S. A.* **2017**, *114*, 1795−1800.
(60) Montoya, J. H.; Shi, C.; Chan, K.; Nørskov, J. K. *J. Phys. Chem. Lett.* **2015**, *6*, 2032−2037.
(61) Goodpaster, J. D.; Bell, A. T.; Head-Gordon, M. *J. Phys. Chem. Lett.* **2016**, *7*, 1471−1477.
(62) Pérez-Gallent, E.; Figueiredo, M. C.; Calle-Vallejo, F.; Koper, M. T. M. *Angew. Chem., Int. Ed.* **2017**, *56*, 3621−3624.
(63) Tang, W.; Peterson, A. A.; Varela, A. S.; Jovanov, Z. P.; Bech, L.; Durand, W. J.; Dahl, S.; Nørskov, J. K.; Chorkendorff, I. *Phys. Chem. Chem. Phys.* **2012**, *14*, 76−81.
(64) Freund, H. J.; Roberts, M. W. *Surf. Sci. Rep.* **1996**, *25*, 225−273.

DOI: 10.1021/acscatal.7b01416
ACS Catal. 2017, 7, 5112−5120